Modeling and Experiments of Voltage Transients of Polymer Electrolyte Membrane Fuel Cells With the Dead-Ended Anode

Serhat Yesilyurt[1]
Sabanci University,
Orhanli, 34956 Tuzla,
Istanbul, Turkey
e-mail: syesilyurt@sabanciuniv.edu

Jason B. Siegel

Anna G. Stefanopoulou

University of Michigan,
Ann Arbor, MI, 48109

Operation of PEM fuel cells (PEMFC) with the dead-ended anode (DEA) leads to severe voltage transients due to accumulation of nitrogen, water vapor and liquid water in the anode channels and the gas diffusion layer (GDL). Accumulation of nitrogen causes a large voltage transient with a characteristic profile whereas the amount of water vapor in the anode is limited by the saturation pressure, and the liquid water takes up very small volume at the bottom of the anode channels in the case of downward orientation of the gravity. We present a transient 1D along-the-channel model of PEMFCs operating with periodically-purged DEA channels. In the model, transport of species is modeled by the Maxwell-Stefan equations coupled with constraint equations for the cell voltage. A simple resistance model is used for the permeance of nitrogen and transport of water through the membrane. Simulation results agree very well with experimental results for voltage transients of the PEMFC operating with the DEA. In order to emphasize the effect of nitrogen accumulation in the anode, we present experimentally obtained cell voltage measurements during DEA transients when the cathode is supplied with pure oxygen. In the absence of nitrogen in the cathode, voltage remained almost constant throughout the transient. The model is used to demonstrate the effect of oxygen-to-nitrogen feed ratio in the cathode on the voltage transient behavior for different load currents. Lastly, the effect of small leaks from the anode exit on the voltage transient is studied: even for leak rates as low as 10 ml/h, nitrogen accumulation in the anode channels is alleviated and the cell voltage remained almost constant throughout the transient according to the results. [DOI: 10.1115/1.4005626]

1 Introduction

The complexity of the balance-of-plant design in PEMFCs is a major drawback that impedes their advance, especially in transportation applications. For example, effective utilization of on-board-stored fuel requires expensive components and advanced mechatronic solutions. A simpler approach to improve fuel utilization, once its shortcomings are addressed, is to operate PEMFCs in the DEA-mode with simple pressure regulators instead of expensive mass flow controllers [1–3]. Major shortcomings of the DEA operation are: first, membrane humidification depends on the product water from the cathode side; second, accumulation of nitrogen dilutes the concentration of hydrogen in anode channels insofar as hydrogen cannot reach to reaction sites uniformly. Along with nitrogen, water vapor accumulates in the anode as well, partially alleviating the first problem, but contributing to the second one. Accumulation of nitrogen and water vapor in the anode blocks hydrogen transport to portions of the active area near the anode exit. Moreover, especially at high current density and relative humidification in the cathode, accumulation of liquid water in the anode-GDL leads to further adverse conditions that render transport of hydrogen difficult throughout the anode [2–6]. Lastly, hydrogen starvation in the PEMFC operating in the DEA mode leads to degradation of the catalyst support through the carbon-corrosion mechanism [7]. Despite all the adverse conditions, operation of PEMFCs with DEA is not well understood and understanding of transport and degradation mechanisms is necessary.

Here, we present a time-dependent one-dimensional along the channel model of DEA transients of PEMFCs between purge cycles. The proposed model is compared with recent experimental results [8] and agrees reasonably well with experimentally measured voltage transients. Experiments and model results show that the cell voltage in the DEA mode decreases with time, first slowly, then rapidly. Depletion of hydrogen in the anode, which is due to accumulation of nitrogen, leads to a slow decay of the cell voltage immediately after the anode exit is closed. As the accumulation of nitrogen continues, hydrogen concentration becomes almost zero in parts of the cell towards the anode exit, and the current generation from the anode reaction almost stops. Thus, the local current density in gradually decreasing portions of the active area with sufficient hydrogen for the anode reaction increases to match the total load current, and results in increased cathode over potential and resistive losses in the cell; hence, the cell voltage decreases at a faster rate than initially observed at the beginning of the transient.

The time-dependent one-dimensional model presented here is described next followed by details of the numerical implementation and simulation results. The model is tuned and verified with the flow-through data first, then validated with voltage measurements of DEA transients presented in Ref. [8]. Furthermore, simulation results are presented to study effects of oxygen-to-nitrogen feed ratio in the cathode and small-leak rates from the anode exit.

2 Description of the Model

Maxwell-Stefan equations are used to calculate concentrations of species along anode and cathode channels, and are coupled

[1]Corresponding author.

Contributed by the Advanced Energy Systems Division of ASME for publication in the JOURNAL OF FUEL CELL SCIENCE AND TECHNOLOGY. Manuscript received September 21, 2011; final manuscript received November 14, 2011; published online March 9, 2012. Editor: Nigel M. Sammes.

Table 1 Model parameters and their values

Parameter	Value
Thickness of the membrane, δ_m	25×10^{-6} m
Effective depth of the anode and cathode channels, $d_{\text{eff}}^{\{an,ca\}}$	$\{12.7,4.69\} \times 10^{-4}$ m
Length of the channels, L	0.073 m
Operation and reference temperatures, $T,\ T_0$	333 and 300 K
Operation and reference pressures, $p,\ p_0$	1.25 and 1 bar
Cathode inlet relative humidity, RH_{ca}	0.6
Cathode inlet stoichiometric ratio	3
Molar volume of the membrane, V_m	0.9×10^{-3} m^3/mole
Concentration of sulfonic groups in the dry membrane, $c_{SO_3}^0$	1200 mole/m^3
Permeance coefficient of N_2, $\psi_{N_2,0}$	1.0×10^{-14} mole/m^2
Reference concentrations of H_2 and O_2, $c_{\{H_2,O_2\}}^{ref}$	{56.4,40} mole/m^3
Electro-osmotic drag coefficient, n_d	$(2.5/22) \times \lambda$
Reference current density at the anode and cathode, $i_{0,ref}^{(an,ca)}$	$\{3 \times 10^4, 6 \times 10^{-3}\}$ A/m^2
Electric resistance of solid parts, R_{solid}	0.3×10^{-4} Ω-m^2
O_2 concentration coefficient, γ_{O_2}	1
H_2 concentration coefficient, γ_{H_2}	1/2
Anode and cathode transfer coefficients, $\beta_{\{an,ca\}}$	{1,1}
Current loss parameter, $J_{\text{loss},0}$	20 A/m^2

with the voltage model to obtain reaction kinetics. Transient effects in the through-plane direction are neglected in the model: resistance models are used for the transport of species in the through-plane direction in gas diffusion layers and the membrane. Equations used in the model are discussed in detail next; numerical values of the parameters used in the model are listed in Table 1.

2.1 Mass Transfer. Maxwell-Stefan equations are used to model the time-dependent transport of species along the anode and cathode channels:

$$\frac{\partial}{\partial t}(\rho w_i) + \frac{\partial}{\partial z}\left(-\rho w_i \sum_j D_{ij}\frac{\partial x_j}{\partial z} + \rho w_i U\right) = r_i \tag{1}$$

where w is the mass fraction, x is the mole fraction, ρ is the density, D_{ij} binary diffusion coefficient of species i and j, z is the coordinate in the direction of the flow, t is time, U is the convective velocity and r is the reaction rate: species in the anode channel are H_2, H_2O vapor and N_2, and in the cathode are O_2, H_2O vapor and N_2. Maxwell-Stefan equations are solved for two species at the anode and cathode; mole fraction (or the mass fraction) of the third component is determined from the conservation of total mass:

$$x_3 = 1 - x_1 - x_2 \tag{2}$$

Binary diffusion coefficients in Eq. (1) are obtained for multicomponent mixtures [9]:

$$D_{ij} = 3.16 \times 10^{-8}\left(\frac{T^{1.75}}{p\left(v_i^3 + v_j^3\right)^2}\right)\left(\frac{1}{M_i} + \frac{1}{M_j}\right)^{1/2} \tag{3}$$

where p is the pressure, v_i the molar volume of species i, T temperature, and M_i the molecular weight of species, i.

In Eq. (1), densities of mixtures in the anode and cathode are obtained from the Dalton's Law:

$$\frac{1}{\rho} = \frac{\sum_i \frac{w_i}{M_i}}{p/(RT)} \tag{4}$$

where R is the universal gas constant.

The convective velocity, U, in Eq. (1) is the average velocity of the flow, and obtained from the summation of velocities that correspond to the exit stoichiometric ratio of the flow and the total flux of the species reacting at the catalyst layer and exchanged through the membrane:

$$U = U_{\text{exit}} + U_{\text{flux}} \tag{5}$$

In the cathode side, the convective velocity is determined from the stoichiometric ratio of the flow, which is usually set to a value sufficiently larger than one. In the anode, the flow of hydrogen, especially near the inlet, is the major part of the convective velocity, since all the hydrogen consumed in the reaction flows through the inlet. The convective velocity due to fluxes of species reacting and crossing over the membrane at a given position is the integral of the sum of downstream mass fluxes:

$$U_{\text{flux}}^{an}(z) = -\frac{1}{\rho_{an}}\int_z^L N_{H_2}^{an}(z') + N_{N_2}^{an}(z') + N_{H_2O}^{an}(z')dz' \tag{6}$$

Here, L is the length of the channels, N_i^{an} inward mass fluxes across the membrane for water vapor and nitrogen, and negative of the mass flux hydrogen reacting at the anode catalyst layer, which is obtained from:

$$N_{H_2}^{an} = -\frac{M_{H_2}}{2F}(J_{\text{cell}} + J_{\text{loss}}) \tag{7}$$

where F is the Faraday's constant, J_{cell} is the local current density and J_{loss} is the parasitic current density due to loss of hydrogen through the membrane to the cathode side. It is assumed that the parasitic loss is proportional to the mole fraction of hydrogen:

$$J_{\text{loss}} = J_{\text{loss},0}x_{H_2} \tag{8}$$

where $J_{\text{loss},0}$ is an estimated constant based on the permeance of hydrogen through the Nafion membrane.

The local flux of nitrogen through the membrane is calculated from the difference between the partial pressures of nitrogen in the cathode and the anode:

$$N_{N_2}^{an} = M_{N_2}\psi_{N_2}\frac{p\left(x_{N_2}^{ca} - x_{N_2}^{an}\right)}{\delta_m} \tag{9}$$

Here, δ_m is the thickness of the membrane, and ψ_{N_2} is the membrane-water-content dependent permeance of nitrogen and given by [2]:

$$\psi_{N_2} = \psi_{N_2}^0\left(0.0295 + 1.21f_V - 1.93f_V^2\right)\exp\left[\frac{E_{N_2}(T - T_0)}{RTT_0}\right] \tag{10}$$

where $\psi_{N_2}^0$ is 1×10^{-14} mole/m^2, E_{N_2} is 24 kJ/mole and f_V is the volumetric ratio of the liquid water in the membrane, and given by:

$$f_V = \frac{\lambda V_{H_2O}}{V_m + V_{H_2O}} \tag{11}$$

Here, λ is the molar ratio of water molecules per sulfonic group in the membrane, V_m and V_{H_2O} are molar volumes of the dry membrane and liquid water.

In Eq. (6), the flux of water vapor across the membrane is calculated from:

$$N_{\mathrm{H_2O}}^{an} = M_{\mathrm{H_2O}}\left[\frac{c_{\mathrm{SO_3}}^{0}\left(\lambda_{eq}^{ca}-\lambda_{eq}^{an}\right)}{R_m} - n_d\frac{J_{\mathrm{cell}}}{F}\right] \tag{12}$$

where $\lambda_{eq}^{(an,ca)}$ is the water content of the membrane at local equilibrium conditions at the anode and the cathode; $c_{\mathrm{SO_3}}^{0}$ is the molar concentration of sulfonic groups in the dry membrane, n_d is the electro-osmotic drag coefficient that gives the number of water molecules dragged by each proton, and R_m is the resistance for water transport across the membrane and given by:

$$R_m = \frac{1}{k_{ads}} + \frac{1}{k_{des}} + \frac{\delta_m}{D_\lambda} \tag{13}$$

In Eq. (13), k_{des} and k_{ads} are the desorption and adsorption coefficients and D_λ is the diffusion coefficient of water in the membrane; k_{des}, k_{ads} and D_λ are experimentally measured by Ge et al. [10] and given by:

$$k_{des} = 4.59\times10^{-5} f_V \exp\left[2416\left(\frac{1}{T}-\frac{1}{T_0}\right)\right] \tag{14}$$

$$k_{ads} = 1.14\times10^{-5} f_V \exp\left[2416\left(\frac{1}{T}-\frac{1}{T_0}\right)\right] \tag{15}$$

$$D_\lambda = 2.72\times10^{-9} f_\lambda \exp\left[2416\left(\frac{1}{T}-\frac{1}{T_0}\right)\right] \tag{16}$$

where f_λ is temperature dependent and specified as:

$$f_\lambda = \begin{cases} 0.0543 + 0.00336\lambda, & T = 323\,\mathrm{K} \\ 0.0771 + 0.00259\lambda, & T = 353\,\mathrm{K} \end{cases} \tag{17}$$

On the cathode-side, the local inward oxygen flux due to the reaction at the catalyst layer is given by:

$$N_{\mathrm{O_2}}^{ca} = -\frac{1}{4F} M_{\mathrm{O_2}}\left(J_{\mathrm{cell}} + J_{\mathrm{loss}}\right) \tag{18}$$

Local inward flux of water vapor on the cathode-side is the sum of the negative of the flux going into the anode and the water coming out from the reaction at the catalyst layer:

$$N_{\mathrm{H_2O}}^{ca} = M_{\mathrm{H_2O}}\left[-c_{\mathrm{SO_3}}^{0}\frac{\left(\lambda_{eq}^{ca}-\lambda_{eq}^{an}\right)}{R_m} + \left(\frac{1}{2}+n_d\right)\frac{J_{\mathrm{cell}}}{F}\right] \tag{19}$$

The nitrogen influx on the cathode-side is the opposite of the flux given by Eq. (9).

In Maxwell-Stefan equations given by Eq. (1), reaction rates are determined from the mass flux of each species given by Eqs. (7), (9) and (12), i.e.:

$$r_i = \frac{N_i}{d_{\mathrm{eff}}} \tag{20}$$

where d_{eff} is the effective depth of the channels and defined as the ratio of the total volume available to species, V_{Total}, and the active area of the fuel cell, A_{cell}, i.e.:

$$d_{\mathrm{eff}}^{an,ca} = \frac{V_{\mathrm{Total}}^{an,ca}}{A_{\mathrm{cell}}} \tag{21}$$

Boundary conditions for Maxwell-Stefan equations in Eq. (1) are specified mass fractions at inlets and outlets of the anode and cathode channels. At the anode inlet, we assume dry hydrogen is supplied during purges as well as dead-ended conditions, i.e.,:

$$\text{At at } z = 0: \quad x_{\mathrm{H_2}} = 1, \qquad x_{\mathrm{N_2,H_2O}} = 0 \tag{22}$$

Similarly to anode-side boundary conditions, at the cathode inlet, mass fractions of the species are specified based on the inlet relative humidity and the pressure. At the anode and cathode exits, fluxes of species are specified as convective fluxes only: i.e. the diffusive fluxes are set to zero:

$$-\rho_i\sum_{j\neq i} D_{ij}\frac{\partial x_j}{\partial z} = 0 \tag{23}$$

The convective flux at the exit, $\rho w_i U$, is nonzero when the inlet stoichiometric flow is specified as greater than one; for the DEA the convective flux at the exit is zero.

2.2 The Voltage Model. We assume that the anode is the ground electrode; then the cathode electrode potential is expressed as the sum of the reversible cell potential, V_{rev}, potential drop in the membrane, $-\Delta V_m$, the anode activation, $-\Delta V_{an}$, and the cathode activation, $-\Delta V_{ca}$, as follows:

$$V_e = V_{rev} - \Delta V_{an} - \Delta V_{ca} - \Delta V_m \tag{24}$$

The reversible cell potential is given by:

$$V_{rev} = V_0 + \frac{RT}{2F}\left[\frac{1}{2}\log\left(\frac{c_{\mathrm{O_2}}}{c_{\mathrm{O_2}}^{ref}}\right) + \log\left(\frac{c_{\mathrm{H_2}}}{c_{\mathrm{H_2}}^{ref}}\right)\right] \tag{25}$$

Here, c_i^{ref} refers to reference concentration of species i, V_0 is the open-circuit potential and given by [11]:

$$V_0 = 1.23 - 0.00083\times(T-298) \tag{26}$$

Anode and cathode activation over potentials in Eq. (24) are given by [12]:

$$\Delta V_{an} = \frac{RT}{F\beta_{an}}\,\mathrm{a\,sinh}\left[\frac{J_{\mathrm{cell}}}{i_{0,ref}^{an}}\left(\frac{c_{\mathrm{H_2}}^{ref}}{c_{\mathrm{H_2}}^{CL}}\right)^{\gamma_{\mathrm{H_2}}}\right] \tag{27}$$

$$\Delta V_{ca} = \frac{RT}{F\beta_{ca}}\,\mathrm{a\,sinh}\left[\frac{J_{\mathrm{cell}}}{i_{0,ref}^{ca}}\left(\frac{c_{\mathrm{O_2}}^{ref}}{c_{\mathrm{O_2}}^{CL}}\right)^{\gamma_{\mathrm{O_2}}}\left(\frac{c_{\mathrm{H^+}}^{ref}}{c_{\mathrm{H^+}}^{CL}}\right)^{\gamma_{\mathrm{H^+}}}\right] \tag{28}$$

In Eqs. (27) and (28), β is the transfer coefficient, γ is the concentration parameter and $i_{0,ref}$ is the reference current density, c_i^{CL} is the concentration of species i in the catalyst layer, and calculated from the resistance model in the GDL:

$$c_i^{CL} = c_i - \frac{\delta_{GDL}}{D_{i,\mathrm{N_2}}} N_i \tag{29}$$

where δ_{GDL} is the thickness of the GDL, $D_{i,\mathrm{N_2}}$ is the binary diffusion coefficient for species i and nitrogen, and N_i is the mass flux.

The last term in the parentheses in Eq. (28) represents the overpotential due to proton deficiency in the cathode catalyst layer. In the DEA operation, there is a severe fuel starvation in parts of the cell, and, hence, the cell current diminishes and the oxygen reaction in the cathode stops as well. We assume that the proton concentration in the cathode remains at equilibrium and does not add to the activation loss.

The potential drop in the membrane is due to ionic resistance of the membrane:

$$\Delta V_m = \frac{\delta_m}{\sigma_m} J_{\text{cell}} \tag{30}$$

where σ_m is the membrane's ionic conductivity and given by an empirical relationship for Nafion membranes [13]:

$$\sigma_m = (-0.326 + 0.514\,\lambda)\exp\left[1268\left(\frac{1}{303} - \frac{1}{T}\right)\right] \tag{31}$$

The cell potential, V_{cell}, at the cathode current collector must be constant, due to high conductivity of the plate, and can be determined from the current density and the total electric resistance of solid components including contacts, R_{solid}; the electric resistance is estimated from the slope of the polarization curve of the cell used in the experiments. The cell potential is, then, obtained from:

$$V_{\text{cell}} = V_e - R_{\text{solid}} J_{\text{cell}} \tag{32}$$

The integral of the current density, J_{cell}, must be equal to the total load current, I_{load}, which is specified as an input in the model, as follows:

$$\int_{A_{\text{cell}}} J_{\text{cell}} dA = A_{\text{cell}} J_{\text{load}} = I_{\text{load}} \tag{33}$$

The unknowns, which are a total of six molar fractions (interchangeably mass fractions) of species, x_i (or w_i), current density, J_{cell}, and the cell potential, V_{cell} are obtained from the solution of the Maxwell-Stefan equations for conservation of mass of individual species, conservation of total mass, coupled with the cell potential and current density equations given by Eqs. (1), (2), (32) and (33), respectively.

3 Numerical Solution

Maxwell-Stefan equations, which are subject to voltage model constraints, are solved numerically with the commercial finite-element package, COMSOL Multiphysics [14]. The constraint equation given by Eq. (24) is represented in the weak form to ensure full coupling between the voltage model and Maxwell-Stefan equations. In the finite-element model, the one-dimensional domain is discretized into 50 linear elements and 301 degrees of freedom.

The steady-state solution is obtained for a flow through operation mimicking the purge-period prior to the DEA transient. In previous experiments, the cell voltage recovered fully during the purge cycles especially for dry operating conditions at the cathode [8]. Therefore, it is assumed that nitrogen and water vapor, which accumulate during the dead-ended transient, are completely removed from the anode channels and GDLs, and that steady-state flow through conditions are restored during the purge cycle.

In order to obtain a converged steady-state solution of the nonlinear equations with Newton-Raphson iterations, the coupling between Maxwell-Stefan equations, cell voltage and current constraints is bootstrapped. First Maxwell-Stefan equations for the anode are solved; then this solution is coupled with Maxwell-Stefan equations for the cathode. Finally, the full set of coupled equations is solved together.

The steady-state solution is used as the initial condition of the dead-ended transient. A variable-step-size maximum third-order backward-difference-formula is used to integrate the discrete system of equations in time with the maximum absolute tolerance of 10^{-4} [14].

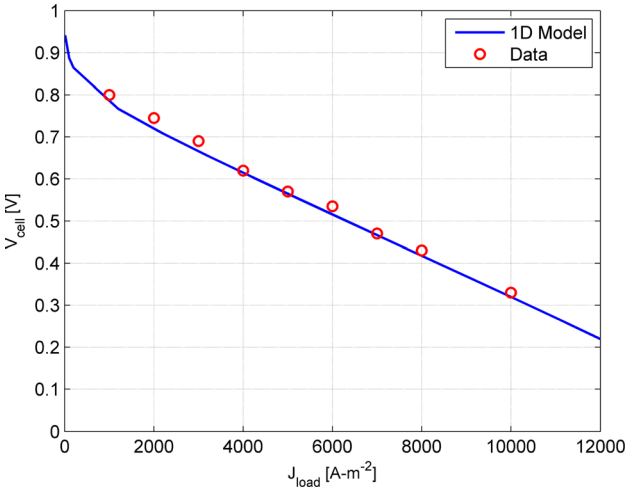

Fig. 1 Comparison of the polarization curves from the experiments reported in Ref. [8], and the model

4 Results

Two of the parameters of the model, the cathode reference current density, $i^{ca}_{0,ref}$, and the electric resistance of the solid components, including the contact resistance, R_{solid}, are obtained from experiment results for steady-state flow-through operation, which are reported in our previous work, [8]. Reference current density and the electrical resistance are influenced by many factors during the construction of the cell such as the electrical contact resistance and catalyst layer deformation due to applied mechanical compression. The polarization curve shown in Fig. 1 verifies the tuning of those parameters in the model.

In Figs. 2 and 3, comparisons of results from experiments and simulations are shown for the cell voltage during DEA transients for $J_{\text{load}} = 3700$ and 5700 A/m^2 respectively. The model-predicted voltage agrees reasonably well with the measured voltages in the experiments for both load current densities.

According to results presented in Figs. 2 and 3, the cell voltage declines at a slow rate for about 400 s into the transient, then the voltage declines at a faster rate; about 4.2 and 15 mV/min for $J_{\text{load}} = 3700$ and 5700 A/m^2 respectively. In our previous work, [8,15], it was shown that the slope of the voltage decline increases when the local hydrogen concentration goes to zero near the exit of the anode channel due to the nitrogen crossover from the

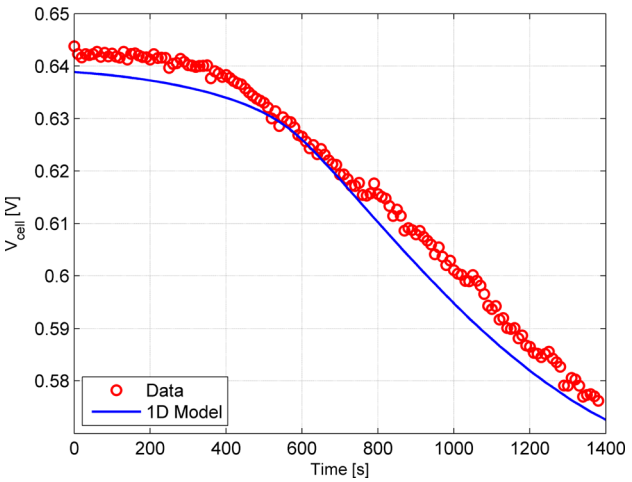

Fig. 2 The voltage transient during the dead-ended operation for $J_{\text{load}} = 3700$ A/m^{-2}

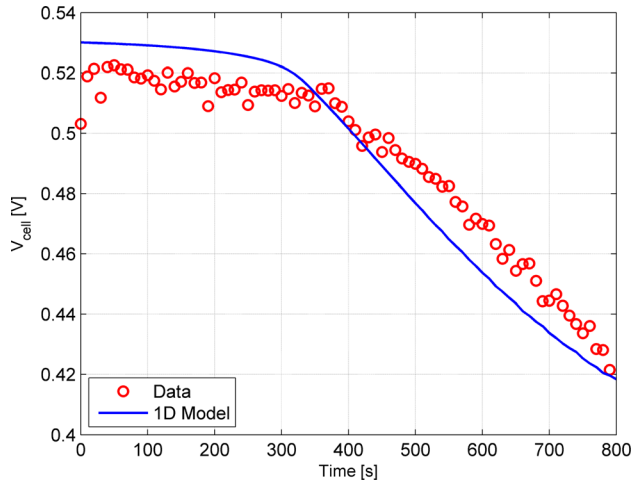

Fig. 3 The voltage transient during the dead-ended operation for $J_{load} = 5700$ A/m^{-2}

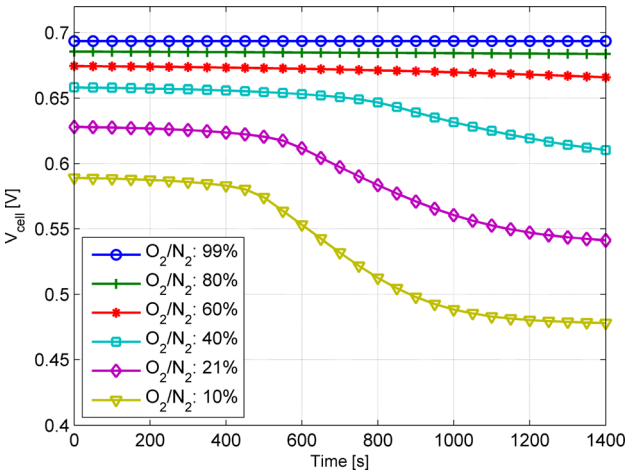

Fig. 5 The effect of the O_2/N_2 ratio on the cell voltage during the DEA transient for $J_{load} = 3700$ A/m^2

cathode to the anode. The size of the effective active area decreases with increasing amount of nitrogen in the anode. During the slow ramp-down, the cell voltage drops because of decreasing hydrogen concentration; during the fast ramp-down, the voltage drops because of increasing effective current density in the portion of the active area where there is sufficient hydrogen for the anode reaction. Due to increased local current density near the inlet of the anode, membrane dry-out is suspected in that region. Local membrane thickness measurements of PEMFCs that operated with periodically purged DEA transients presented in Ref. [17] confirm that the membrane thickness is reduced in parts of the cell where the maximum local current densities are expected.

In experiments presented in Ref. [8], a solenoid valve downstream from the anode exit is used to close the anode exit. The part of tubing between the actual exit of the anode channels and the valve may act as a reservoir and allow some nitrogen to travel into the available volume in the tubing. In order to mimic the flow of nitrogen into the tubing before the solenoid valve, small leak rates are specified at the anode exit, 0.23 ml/h (corresponding stoichiometric ratio is 0.0001) for $J_{load} = 3700$ A/m^2 and 0.17 ml/h (corresponding stoichiometric ratio is 0.00005) for $J_{load} = 5700$ A/m^2, respectively, in the model.

4.1 The Effect of the Oxygen-to-Nitrogen Ratio. The utmost importance of the nitrogen crossover from the cathode to dead-ended anode is demonstrated with experiments, in which air on the cathode side is replaced with pure oxygen. In experiments, an identical cell to the one reported in Ref. [8] is used. The cell operated with the load current density of 4000 A/m^2, cathode inlet relative humidity of 0.8 and with DEA transients that take 2100 s between purges. After the initial cycle with a 15 mV drop in the cell voltage, the cell voltage remained within 5 mV in subsequent cycles as shown in Fig. 4. The cell voltage remained unaffected by dead-ended transients for load current densities 6000 and 8000 A/m^2 as well (not shown here). The range of the transients observed in the cell voltage, as shown in Fig. 4, exhibits a similar behavior to the transients with the air flow in the cathode in a much smaller scale, 10 mV versus 50–100 mV. The small transient may take place due to the accumulation of water vapor and liquid water, which is not clearly understood here.

A number of transient simulations are carried out to study the effect of the oxygen-to-nitrogen feed ratio on the cell voltage during the dead-ended operation of the cell. In the simulations, the cathode stoichiometric ratio is set to 3, unless the cathode velocity is below 1 m/s. In Figs. 5 and 6, the cell voltage transients are shown for a number of oxygen-to-nitrogen ratios in the cathode for $J_{load} = 3700$ and 5700 A/m^2, respectively. Consistently with the experiments with pure oxygen in the cathode, the cell potential

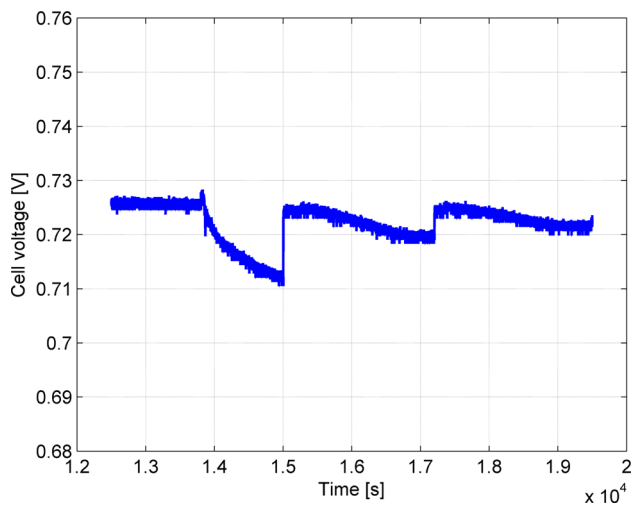

Fig. 4 Voltage transient during the dead-ended operation with pure oxygen in the cathode for $J_{load} = 4000$ A/m^2

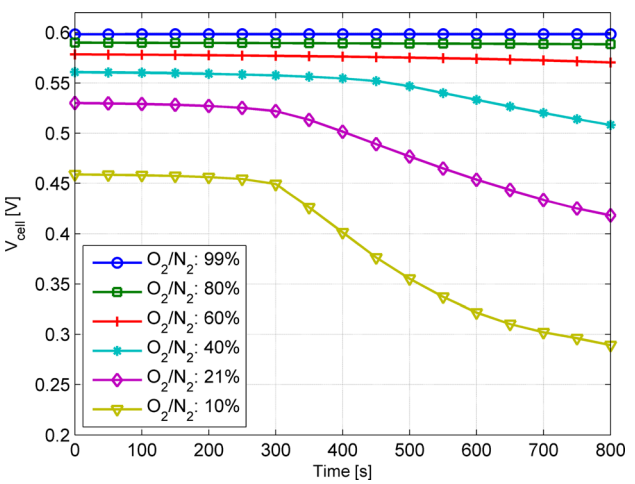

Fig. 6 The effect of the O_2/N_2 ratio on the cell voltage during the DEA transient for $J_{load} = 5700$ A/m^2

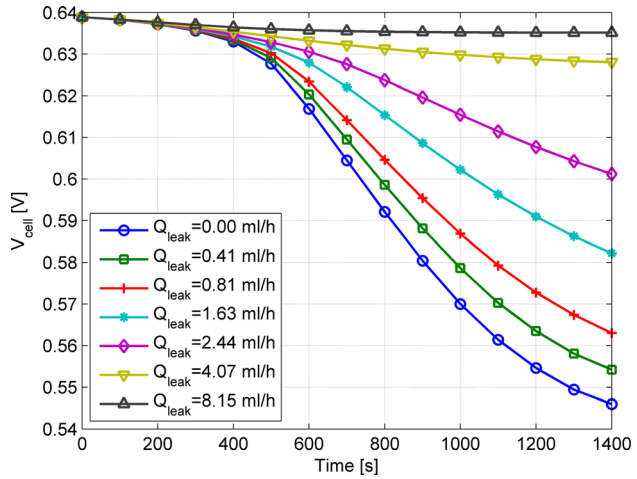

Fig. 7 The effect of the anode exit leak on the cell voltage during the dead-ended transients for $J_{load} = 3700$ A/m^2

varies very little when the oxygen-to-nitrogen ratio in the cathode is very high. As the ratio is reduced, the double-sloped response of the cell voltage is observed during transients. Furthermore, regardless of the magnitude of the load current, the duration of the slow ramp-down of the cell voltage decreases as the oxygen-to-nitrogen ratio increases.

4.2 The Effect of the Anode Exit Leak. Transient simulations are carried out with a number of leak rates specified at the anode exit in order to demonstrate the effect of nitrogen accumulation. In Fig. 7, the cell voltage transients are shown for exit leak rates of 0, 0.41, 0.81, 1.63, 2.44, 4.07 and 8.15 ml/h and for $J_{load} = 3700$ A/m^2. Total drop in the voltage decreases with increasing leak rate from about 90 mV with no leak at the exit to 3.8 mV for a leak rate of 8.15 ml/h, which corresponds to an ultra low exit stoichiometric ratio of 0.001 at the anode. In Fig. 8, cell voltage transients are shown for leak rates of 0, 0.63, 1.26, 2.51, 3.77 and 6.28 ml/h for $J_{load} = 5700$ A/m^2. The cell voltage drop at the end of 800-s transient is 82 mV when there is no leak and only 7 mV when there is a leak as low as 6.28 ml/h at the exit corresponding to stoichiometric ratio of 0.0005.

According to simulation results shown in Figs. 7 and 8, the initial response of the cell voltage remains almost identical for all leak rates. At the beginning of the transient, as long as the leak rate is small, the accumulation of nitrogen in the anode does not vary the distribution of hydrogen insofar as the voltage transient is concerned. As the leak rate increases, nitrogen coming to the anode is discharged and the rate of cell-voltage decline decreases.

In order to effectively restore the cell voltage that tends to decline with the accumulation of nitrogen, the leak rate at the anode exit must be high enough to discharge all nitrogen from the anode and must be low enough to preserve the fuel and water vapor in the anode. For example, for $J_{load} = 3700$ A/m^2, total rate of nitrogen accumulation in the anode is about 3.5 ml/h from a simple calculation using Eqs. (9) and (10). Thus, clearly, leak rates as low as a few mili-liters-per-hour will be enough to discharge nitrogen and ensure somewhat uniform distribution of hydrogen in the active area.

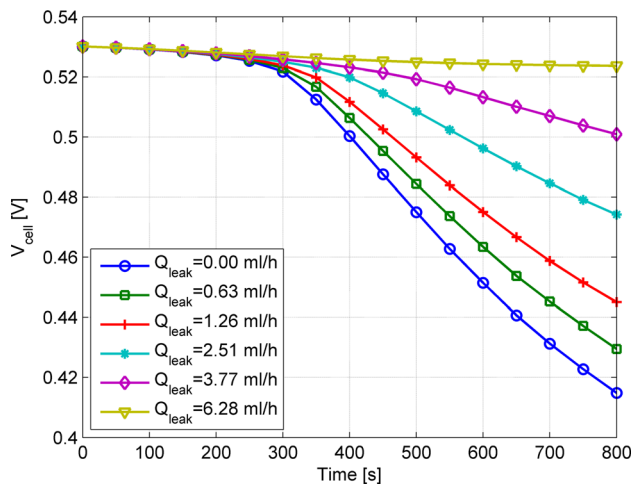

Fig. 8 The effect of the anode exit leak on the cell voltage during the dead-ended transients for $J_{load} = 5700$ A/m^2

5 Conclusion

The time-dependent one-dimensional (in the flow direction) model of the PEMFC operating with periodically-purged dead-ended anode channels is presented here. For verification and calibration, two parameters of the model are tuned with the flow through experiments of the PEMFC that is used for the dead-ended transient experiments as well: namely, the reference current density in the cathode and the electrical resistance of the solid components including the contact resistance are set. In order to validate the model, simulations of dead-ended transients for two load current densities, 3700 and 5700 A/m^2 are compared with experiments: voltage transients during the DEA operation agree very well with experimental results.

In order to study the effect of nitrogen accumulation in the voltage response during the transients, experiments are conducted with pure oxygen in the cathode. The cell voltage effectively remains unaffected during the DEA transient, confirming the effect of the nitrogen accumulation in the anode on the voltage decline. In order to study the effect of the oxygen-to-nitrogen ratio in the cathode on the cell voltage during the DEA transient, the model is used to conduct further simulations. Cell-voltage drop in the DEA transient decreases as the oxygen ratio is increased in the cathode feed.

Lastly, the effect of the anode exit leak (on the order of a few ml/h's) is studied with the model. The simulation results show that a leak rate of less than 10 ml/h is sufficient to discharge the most of accumulated nitrogen from the anode, and to keep the cell voltage nearly flat during the DEA transient.

Acknowledgment

This work was supported by The Scientific and Technological Research Council of Turkey, TUBITAK-MAG 109M105, and the National Science Foundation through CBET-0932509.

References

[1] Karnik, A. Y., Sun, J., and Buckland, J., 2006, "Control Analysis of an Ejector based Fuel Cell Anode Recirculation System," Proceedings of American Control Conference, Minneapolis, MN, June 2006, pp. 484–489.
[2] Ahluwalia, R. K., and Wang, X., 2007, "Buildup of Nitrogen in Direct Hydrogen Polyner-Electrolyte Fuel Cell Stacks," J. Power Sources, **171**, pp. 63–71.
[3] Muller, E. A., Kolb, F., Guzzela, L., Stefanopoulou, A. G., and McKay, D., 2010, "Correlating Nitrogen Accumulation with Temporal Fuel Cell Performance," J. Fuel Cell Sci. Technol., **7**(2), p. 021013.
[4] Kocha, S. S., Yang, J. D., and Yi, J. S., 2006, "Characterization of Gas Crossover and its Implications in PEM Fuel Cells," AIChE J., **52**(5), pp. 1916–1925.
[5] Weber, A. Z., 2008, "Gas-Crossover and Membrane-Pinhole Effects in Polymer Electrolyte Fuel Cells," J. Electrochem. Soc., **155**(6), pp. B521–B531.
[6] Siegel, J. B., McKay, D. A., Stefanopoulou, A. G., Hussey, D. S., and Jacobson, D. L., 2008, "Measurement of Liquid Water Accumulation in a PEMFC with Dead-Ended Anode," J. Electochem. Soc., **155**(11), pp. B1168–B1178.
[7] Raiser, C. A., Bregoli, L., Patterson, T. W., Yi, J. S., Yang, J. D., Perry, M. L., and Jarvi, T. D., 2005, "A Reverse-Current Decay Mechanism for Fuel Cells," Electrochem. Solid-State Lett., **8**(6), pp. A1432–1442.
[8] Siegel,J. B., Bohac, S. V., Stefanopoulou, A. G., and Yesilyurt, S., 2010, "Nitrogen Front Evolution in Purged Polymer Electrolyte Membrane Fuel Cell with Dead-Ended Anode," J. Electochem. Soc., **157**(7), pp. B1081–B1093.

[9] Bird, R. B., Stewart, W. E., and Lightfoot, E. N., 2002, *Transport Phenomena*, 2nd ed., Wiley, New York.
[10] Ge, S., Li, X., Yi, B., and Hsing, I-M., 2005, "Absorption, Desorption, and Transport of Water in Polymer Electrolyte Membranes for Fuel Cells," J. Electrochem. Soc., **152**(6), pp. A1149–A1157.
[11] Barbir, F., 2005, *PEM Fuel Cells: Theory and Practice*, Academic Press, New York.
[12] Newman, J., and Thomas-Alyea, K. E., 2004, *Electrochemical Systems*, 3rd ed. John Wiley & Sons, New York.
[13] Springer, T. E., Zawodzinski, T. A., and Gottesfeld, S., 1991, "Polymer Electrolyte Fuel Cell Model," J. Electrochem. Soc., **138**(8), pp. 2334–2342.
[14] COMSOL, 2010, "COMSOL Multiphysics User Guide," COMSOL A. B., Stockholm, Sweden.
[15] Siegel, J. B., Stefanopoulou, A. G., and Yesilyurt, S., 2010, "Modeling and Simulations of PEMFCs Operating with Periodically Purged Dead Ended Anode Channels," Proceedings of the ASME 2010 Eighth International Fuel Cell Science, Engineering and Technology Conference, June 2010.
[16] Benziger, J., Kimball, E., Meija-Ariza, R., and Kevrekidis, I., 2011, "Oxygen Mass Transport Limitations at the Cathode of Polymer Electrolyte Membrane Fuel Cells," AIChE J., **57**(9), pp. 2505–2517.
[17] Matsuura, T., Siegel, J. B., Chen, J., and Stefanopoulou, A. G., 2011, "Multiple Degradation Phenomena in Polymer Electrolyte Fuel Cell Operation with Dead-Ended Anode," Proceedings of the ASME 2011 9th Fuel Cell Science, Engineering and Technology Conference, FuelCell2011, August 7–10 2011, Washington DC, USA.